ISSN 1330-3651 (Print), ISSN 1848-6339 (Online)
https://doi.org/10.17559/TV-20220105203656
Original scientific paper

A New Soft-Switching Control Technique and Loss Analysis for Parallel Resonant DC-Link Inverter Connected to the Grid

Hakan DONUK*, Bilal GUMUS

Abstract: This study is recommended to develop a soft-switching control software infrastructure that enables more efficient and effective use of parallel resonant DC link circuits. The fact that the control technique can be easily applied to the soft switching circuit makes it important in this field. With this proposed study, lower voltage ripple and higher efficiency are obtained. To see the results of the technique and to study its effect, a study was carried out on a grid connected inverter. When the frequency changes between 5-15 kHz and 5-10 kW power is transmitted to the grid, the soft switching effect is studied and the efficiency is increased. A software model for calculating the power losses of semiconductor switches has also been established. Using this modeling approach, the power consumption is calculated in detail and the loss analysis is performed using catalog data of semiconductor switches. The accuracy of the obtained results was compared with another simulator. While the PRDCL inverter using the new proposed switching technique transmits 10 kW of power to the grid, the efficiency increased from 97.67% to 98.61% at a switching frequency of 5 kHz, from 96.82% to 98.58% at a switching frequency of 10 kHz, and from 95.61% to 98.55% at a switching frequency of 15 kHz.

Keywords: active power filter; hard switching; parallel resonant dc link; power loss calculation; soft switching

1 INTRODUCTION

Today, many areas of the power electronics industry benefit from inverters. In addition to motor drivers, APFs, grid-connected synchronous power systems, and renewable energy applications, these are areas where inverters are actively used. The importance of inverters working in shunt with the grid, which plays a major role in power transmission, is increasing day by day. With the widespread use of alternative energy sources, transmission of the generated energy obtained to the grid is preferred over storage as it is a more economical solution. Inverters are also required to use the energy stored in energy storage devices in AC systems. In the development of microgrid architectures and smart grid structures, inverters have a greater responsibility in ensuring energy continuity. The maximum degree of energy transfer to the grid is related to the high efficiency of the inverters used. Parameters such as total current harmonic distortion of current (THDi), PF of generated power, modulation technique of inverter, grid synchronization and low switching losses are important factors that determine the quality of inverter systems operating in synchronization with the grid [1-3]. Grid synchronization is a very important problem in distributed power generation systems. Synchronization with the grid and power control are done by determining the angle of the grid voltage vector using algorithms and switching the inverter according to this angle value. Grid synchronization is achieved using certain methods such as zero crossing method, *α-β* filter method, *d-q* filter method, *d-q* PLL method and adaptive PLL method [4-8].

In converters, efficiency is increased by reducing switching losses of semiconductor elements. Many methods have been developed to eliminate or reduce switching losses. Basic soft switching methods used to improve converter quality: ZCS, ZVS, ZCT, and ZVT. Soft switching control in DC-DC converters is simple and easy due to the characteristics such as unidirectional power flow and constant switching frequency. In DC-AC systems with bidirectional power flow and two frequencies, one of which is fundamental and the other variable, soft switching is relatively more difficult and complex than in DC-DC converters. There are many structures in the literature to increase the efficiency of inverters [9]. Among them, the RPI is known for its easy-to-understand control structure, low voltage ripple, and no need for an additional switch, and is designed for high and medium power. The negative aspects of this structure are that the resonant pole inverter requires a separate resonant circuit structure for all of its legs and incurs relatively more energy losses compared to other topologies [10]. The zero- voltage transition PWM inverter ZVTI, which operates in discontinuous transmission with diode and realizes the soft switching function with the help of an additional switch, reduces the switching losses, but it cannot show the same effect at low loads [11]. In the basic RDCLI structure where DPM is used, no active switches are used. Voltage free transitions are achieved by ensuring continuity at resonance with proper control of power elements. The fact that PWM technique cannot be used in this structure, voltage fluctuations in DC part of the inverter and current fluctuations on the inductor are presented as disadvantages [12].

In the passive suppressed resonance transition structure DC, where the transformer is actively involved in the resonance event, the switches are under ZVS, while their turn off occurs under ZCS. The long duration of the zero-voltage process causes very high currents to flow through the inductor. Undesirably high currents cause both high losses and high voltage fluctuations on the capacitor side. In the DC link inverter structure, two active switches with parallel resonance transition are used to provide smooth switching only when the inverter switches turn on. According to the PWM control algorithm, the inverter switches that need to be transmitted are turned on simultaneously, but each switch is smoothly removed from the transmission thanks to separate suppression capacitors [13].

Two auxiliary active switches and a transformer are used in the QRDCL structure to enhance the performance of active power filters designed to eliminate harmonics [14]. In the active power filter, hard switched inverter switches can be soft switched by using a suitable switching technique with PWM control. The general problem of soft switched resonant converters using pulse width modulation is that they are subjected to high inductor currents and can provide smooth switching conditions only in limited power

ranges. To overcome these problems, a new hybrid modulation technique for series resonant inverters has been proposed. Apart from the complexity of the control structure, experimental studies confirmed that the general problems were overcome [15]. In reference [16], where a soft-switching structure is provided by using fewer elements for the three-phase inverter, the auxiliary circuit is controlled using the soft-switching technique similar to the traditional PWM method, and in this topology where a single active auxiliary switch is used, the control of the switch is operated according to a certain algorithm.

In soft switching topologies proposed for inverter structures, there are problems such as high voltage or current fluctuations, high currents in inductor leading to large load on capacitor, power range is limited and soft switching control technique is complex. PRDCL topology has been proposed for inverters where these problems are minimized. However, in these inverters, the most suitable soft switching technique should be selected to perform the soft switching operation in a healthy and safe manner [17]. For PRDCL inverters, the thresholds of resonant inductance or capacitance should be adjusted to apply the switching technique properly. This necessity brings the need for a complex control structure [18-20]. For this reason, the control of inverters in auxiliary circuits created with fewer elements is simpler and less complicated [21].

To calculate the efficiency of switching power supplies with high accuracy, the energy consumed by solid state power switches should be calculated in detail. Some analytical methods have been developed in the literature to measure the power dissipation of semiconductor switches. Some efficiency calculations can be performed using the data sheets of semiconductor power devices provided by the manufacturers. With the current-voltage loss curves given in the data sheet, the switching and conduction losses consumed in the internal structure of a semiconductor switch can be calculated in detail for any frequency and loss analysis can be performed [22-24]. In this paper, the physical model of the PRDCL structure with a grid-connected inverter was created using Simscape real element models in Matlab/Simulink and the proposed switching technique was applied to the PRDCL structure. Detailed calculations of power losses and efficiency of inverter switches were performed using an algorithm prepared in Matlab/Simulink and the accuracy of the calculation was compared with the simulator developed by the manufacturers for their products.

The focus of this study is to propose the developed PRDCL structure for inverters to the grids and reduce the switching losses in the inverter by developing a new switching control technique for PRDCL. The purpose of the switching control technique is to match the on and off timing of the inverter switches during grid application when the dc bus is at zero voltage level. In this way, efficiency is increased by reducing the losses of the switches that are turned on at zero voltage. In the switching control proposed for PRDCL circuit, no additional circuit is required but it is implemented using digital logic gates. Since the control technique is activated after PWM pulses are generated, it also works in accordance with other types of modulation and can be used in microgrids, active power filters, switching power supplies and distributed static compensators.

2 DESCRIPTION AND DESIGN OF PARALLEL RESONANT DC LINK INVERTER

The parallel resonant DC link structure consists of three semiconductor switches and a parallel resonant circuit, as shown in Fig. 1. The expected resonance event between inductor and capacitor is achieved by the S_{Y1} and S_{Y2} switches. The S_s switch plays an active role in lowering the DC bus to zero voltage level. By selecting and applying the proper soft switching technique in the PRDCL structure, zero voltage switching can be achieved by lowering the bus voltage to zero without causing voltage or current stresses in the inverter switches. The smooth switching affects both the inverter switches and the auxiliary switches. Since the zero voltage transition in the circuit can be controlled by switching techniques, this can also increase the PWM capability [17].

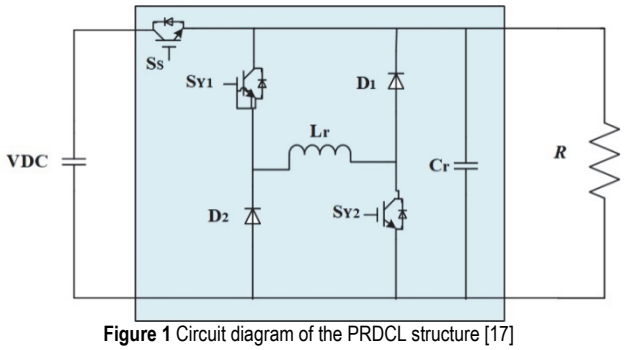

Figure 1 Circuit diagram of the PRDCL structure [17]

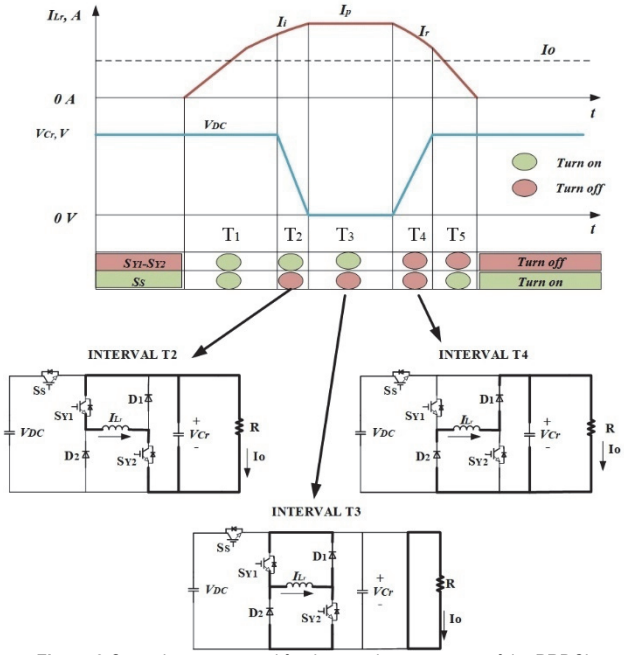

Figure 2 Operating ranges and fundamental wave curves of the PRDCL

PWM pulses are obtained by comparing a saw wave to a sine wave with a phase angle of 120°. Before the resulting inverter gate pulses are applied to the switches, the soft switching process for the main switches must be prepared in a safe and sound manner. As shown in Fig. 1, two of the three active switches (S_{Y1} and S_{Y2}) belonging to the auxiliary circuit receive the same gate signal, while the gate signal of the other (S_S) is generated separately. In order to theoretically explain and simplify the operation of the circuit, several assumptions have been made. It is assumed

that all elements are considered ideal, the resonant inductance is chosen sufficiently larger than the load inductance, the output load is represented by a simple resistor *R,* and there is no DC bus voltage ripple. There are six different ranges in the operation of the auxiliary circuit. Resonance current voltage graphs regarding this range and the operation of the circuit are shown in Fig. 2 and detailed in reference [17].

Resonant frequency/characteristic impedance and circuit equations:

$$\omega_r = 1/\sqrt{L_r \cdot C_r} \tag{1}$$

$$Z_r = \sqrt{L_r / C_r} \tag{2}$$

In steady state mode (S_S: on, S_{Y1}-S_{Y2}: off):

$$i_{Lr}(t) = 0 \tag{3}$$

$$v_{Cr}(t) = V_{\mathrm{DC}} \tag{4}$$

In the T_1 interval (S_S: on, S_{Y1}-S_{Y2}: on):

$$i_{Lr}(t) = \frac{V_{\mathrm{DC}}}{L_r} t \tag{5}$$

$$v_{Cr}(t) = V_{\mathrm{DC}} \tag{6}$$

$$T_1 = \frac{L_i \cdot I_i}{V_{\mathrm{DC}}} \tag{7}$$

In the T_2 interval (S_S: off, S_{Y1} - S_{Y2}: on); this operating range is the first resonance region. The switch S_S is deactivated at zero voltage and the resonance process starts with the offset current I_o. In this case, the resonance current and voltage of the resonance capacitor can be written as follows:

$$i_{Lr}(t) = \frac{V_{\mathrm{DC}}}{Z_r}\sin(\omega_r t) + (I_i + I_o)\cos(\omega_r t) - I_o \tag{8}$$

$$v_{Cr}(t) = V_{\mathrm{DC}}\cos(\omega_r t) - (I_i + I_o)\sin(\omega_r t) \tag{9}$$

$$T_2 = \frac{1}{\omega_r}\tan^{-1}\left(\frac{V_{DC}/Z_r}{I_i + I_o}\right) \tag{10}$$

Maximum resonant current (I_p):

$$I_p = i_{Lr}(T_2) = \sqrt{(I_i + I_o)^2 + \left(\frac{V_{\mathrm{DC}}}{Z_r}\right)^2} - I_o \tag{11}$$

In the T_3 interval (S_S: off, S_{Y1} - S_{Y2}: on); this operating region is the free-circulation range, and the inductor current circulates freely through I_{Lr}, S_{Y1} - D_1, and S_{Y2} - D_2. During this time, the voltage of the resonant capacitor VCr is kept at zero. This zero voltage range forms the ZVT environment for the switching elements in the inverter. The duration of this zero voltage interval (T_3) can be controlled by the PWM signal applied to switches S_{Y1} and S_{Y2}. In this case, the resonance current and the capacitor voltage:

$$i_{Lr}(t) = I_p \tag{12}$$

$$v_{Cr}(t) = 0 \tag{13}$$

In the T_4 interval (S_S: off, S_{Y1} - S_{Y2}: off); this operating range is the second resonance range. After changing the switch settings in the inverter, switches S_{Y1} and S_{Y2} are deactivated under zero voltage conditions and the capacitor voltage is recharged to V_{DC} voltage. The new path of the inductor current is D_1, D_2 and Cr. The capacitance voltage v_{Cr} reaches V_{DC} voltage by resonance. In this case:

$$i_{Lr}(t) = (I_p - I_{ox})\cos(\omega_r t) + I_{ox} \tag{14}$$

$$v_{Cr}(t) = Z_r(I_p - I_{ox})\sin(\omega_r t) \tag{15}$$

$$T_4 = \frac{1}{\omega_r}\sin^{-1}\left(\frac{V_{\mathrm{DC}}/Z_r}{I_p - I_{ox}}\right) \tag{16}$$

$$I_p = i_{Lr}(T_4) = \sqrt{(I_p - I_{ox})^2 - \left(\frac{V_{\mathrm{DC}}}{Z_r}\right)^2} + I_{ox} \tag{17}$$

In the T_5 interval (S_S: on, S_{Y1} - S_{Y2}: off):

$$i_{Lr}(t) = -\frac{V_{\mathrm{DC}}}{L_r} t + I_r \tag{18}$$

$$v_{Cr}(t) = V_{\mathrm{DC}} \tag{19}$$

$$T_5 = \frac{L_r \cdot I_r}{V_{\mathrm{DC}}} \tag{20}$$

It is given with equations. With the resonant inductance (Lr) connected in the middle of the circuit, the resonant capacitor (Cr) composes the parallel resonant circuit. The soft transition of the switches depends on the healthy and safe occurrence of the resonance event.

3 MODELING AND LOSS ANALYSIS OF A GRID-CONNECTED PRDCL INVERTER IN MATLAB/SIMULINK

3.1 Inverter Current Control and Grid Synchronization

In order to transfer the energy generated from alternative energy sources to the power grid, it must be converted from DC to AC. This conversion process is done with devices called inverters, with three-phase inverters being used for high-power applications. Since inverters are expected to produce high quality power since they transmit power to the grid, grid currents should not exceed the limit values according to IEEE 519-1992 standards [25]. The important parameters that determine the quality of the grid are the purity of the grid from disturbances, the currents generated at the inverter output that are close to sinusoidal and have the same phase angle with the corresponding

phase voltages. With proper control of the inverter current and grid synchronization, high quality power transmission to the grid is ensured. In grid-connected inverters, there are generally two control loops. Due to the simplicity of controlling the *d-q* components, the algorithm of this control system was created in Matlab/Simulink and its hardware-supported implementation was also done in the loop [26]. These are the internal current control loop, which controls the grid current, and the external voltage control loop, which controls the DC bus voltage and reactive power. The harmonic elimination and dynamic response of the system are controlled by the current control loop and the power flow balance is controlled by the voltage control loop [27, 28].

3.2 Proposed Soft Switching Control Technique and Design Consideration

In this section, a new switching technique is described to smoothly switch the switches of a parallel resonant DC-link. The proposed switching technique is based on the idea that the switches operate under zero voltage by delaying the main PWM pulses and detecting the turn-on and turn-off points of the main inverter switches in advance, and reducing the DC bus voltage to zero at these times. As shown in Figs. 3 and 4, the inverter gate pulses obtained by any modulation method must be delayed by a certain time (*Tdelay*) before being applied to the switches to prepare the soft switching environment in a safe and healthy manner. The delay time can be varied to control switching on or off. Delay blocks are used for both PWM main pulses and auxiliary switch delay S_S.

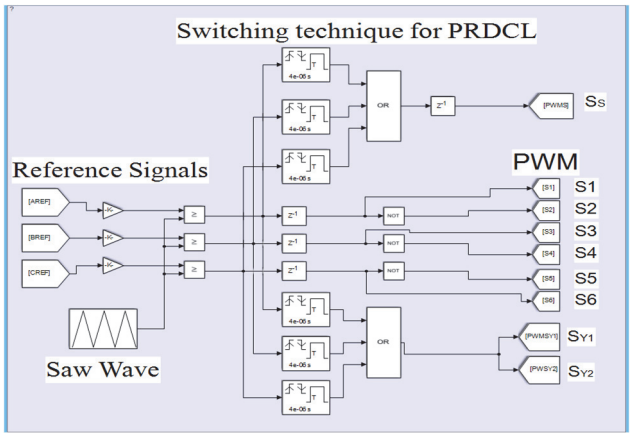

Figure 3 Digital block diagram of the proposed switching control technique

The main switches of the inverter are shifted by a certain time with delay blocks to gain time for the zero-voltage environment. The signals from the main switches are acquired with monostable blocks and all the signals are collected in logic gates. Since the monostable block can control the rising or falling edge conditions of the main signals, the moments when the switch enters the on or off state can be detected. When the pulses of the main switch gates change, this situation is detected in the logic circuit and the auxiliary switches are controlled by logic gates and the DC link voltage is reduced to zero by resonance. When the switching technique is applied to the auxiliary circuit, while the S_S breaker maintains its state in the on state, the S_{Y1}-S_{Y2} breakers are switched to the on state in the off state and thus the first resonance process starts. Depending on the value of the resonance process, a delay block is placed between S_S and the S_{Y1} - S_{Y2} gate pulses. During the resonance process, when the *Lr* element reaches a certain value during the charging process, the series switch S_S is switched to the off state with a certain delay and the connection between the DC link and the inverter is disconnected.

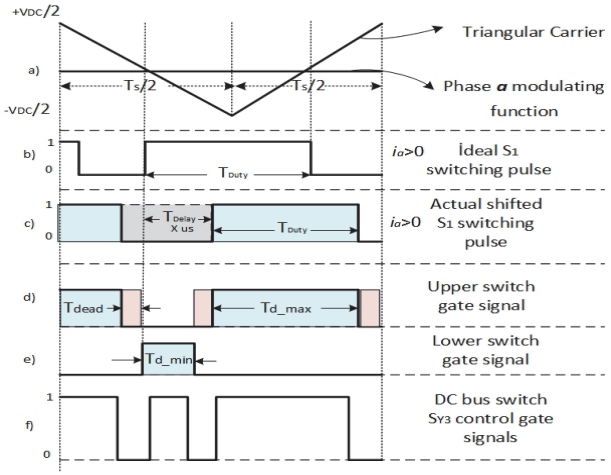

Figure 4 Graphs of application of dead and delay times to control technique

Therefore, in order for the soft switching PRDCL process to be operated in a controlled act, some design criteria must be calculated beforehand. The first criterion is that the resonant inductance current (I_p) must be large enough to drive the capacitor voltage V_{Cr} back to V_{DC}.

$$I_p \geq \frac{V_{\mathrm{DC}}}{Z_r} + I_{ox} \tag{21}$$

where, next load current I_{ox} can be predict from the next switching patterns [29] as

$$I_{ox} = S_1 \cdot I_a + S_2 \cdot I_b + S_3 \cdot I_c \tag{22}$$

As in other resonant structures, the pulse width is restricted in the PRDCL structure. Assuming the current I is properly controlled, then the minimum pulse width $T_{w\min}$ under the worst conditions can be obtained from the equation below.

$$T_{w\min} = \frac{2L_r}{V_{\mathrm{DC}}} \sqrt{I_{o\max}\left(\frac{V_{\mathrm{DC}}}{Z_r} + I_{o\max}\right)} \tag{23}$$

The second important criterion is that the voltage drops to zero from the start time of the first resonance is the minimum value of the duration T_2. The V_{DC} voltage drops to zero with resonance, the switches must be completed before repositioning. That is, the resonance operation of key transitions should already start with the $T_{2\min}$ time. This means the synchronization of the resonance operation with the PWM makes it possible to achieve ZVT safely. As the capacitor *Cr,* which is at the voltage level DC, decreases toward zero level, the inductor *Lr* is charged and reaches its maximum value. The zero level of the capacitor voltage provides a soft switching environment for the main

switches. Thus, when the voltage is zero, the switch is provided softly for the transition. After the main switch transitions to the on state, the auxiliary switches S_{Y1} - S_{Y2}, which are still in the on position, transition to the off state as their conduction time expires. The energy in the *Lr* inductor decreases and starts charging the *Cr* capacitor with resonance. When the resonant capacitor reaches the DC voltage level, the SS series switch goes back to the on state and returns to its original position. This process is repeated when all the switches of the inverter are turned on. The switching technique provides smooth switching for all semiconductor elements. No additional active or passive elements are required in the PRDCL structure to apply this technique. By applying the technique, no unexpected voltage fluctuations occur at the switches. With this technique, the duration of the zero voltage generated to turn the switches on or off can be controlled by the user. The structure of digital circuit is simple and easy to control, and due to its programmable feature, DSP, FPGA, etc., it can be used in processors. It can be easily used in processors.

3.3 Switching Loss Calculation

The extent to which the new switching technology applied to the PRDCL inverter operating on the grid will result in energy savings for the switches can only be determined by loss analysis. In order to obtain and analyse loss energy data in detail, the switching losses (switching losses on and off) of each IGBT switch must be decomposed. In this section, in addition to the studies on analytical calculation of switching losses in the literature, a model prepared in Matlab /Simulink is presented. In the prepared model, the equations of current-voltage curves and loss curves contained in the datasheet of the selected semiconductor elements were linearized and redrawn in Matlab. The equations resulting from the new curves can be used to determine the instantaneous losses in the desired frequency and power range. A detailed Simulink block representation of the switching loss calculation model can be found in Fig. 5. The loss calculation block consists of units for the decomposition, equation, and switching time acquisition. First, the current composition of the IGBT and the diode connected in parallel is decomposed as a function of the current direction. The power consumption is determined by classifying the current data and fitting it into curve equations created for each semiconductor element.

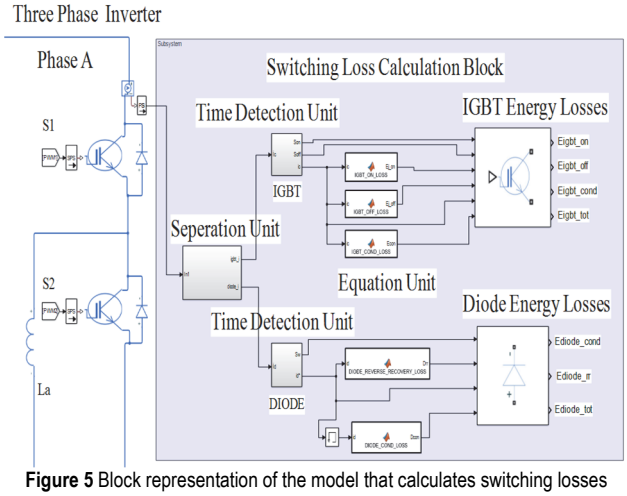

Figure 5 Block representation of the model that calculates switching losses

The instantaneous turn on and turn of times of the switches and diodes of the inverter operating at a given frequency are determined, and the energy losses are obtained by multiplying them by the predetermined power consumption. Thus, the individual switching losses for both the IGBT switch and the diode can be determined. As shown in Eq. (24), conduction and switching energy losses occur in semiconductor elements such as IGBT and diode.

$$E_{\text{tot}} = E_{\text{cond}} + E_{\text{sw}} \tag{24}$$

When operating below a certain frequency, the IGBT elements in the inverter turn on in the positive intervals of the fundamental period, connected to a three-phase system. In the negative region, while the reverse diode connected in parallel turns on, the IGBT goes into turn off. When calculating the conduction loss of a switch, Eq. (24) must be considered only during the positive period, while the conduction loss of the diode must be considered only during the negative period. As can be seen in Eq. (25), the conduction loss is calculated by taking the integral of the energy consumed during the transmission period in a switching period.

$$E_{\text{cond}} = \int_{\text{Ton}(k)} V_{\text{CE}}(t)\, i_{\text{C}}(t)\, \text{d}t \tag{25}$$

In this equation, V_{CE} and i_{C} respectively represent the saturation voltage and collector current of the IGBT switch, while the parameter k represents the switching number. The switching losses of the semiconductor element are also classified within itself. The energy losses occurring during the turn on and turn off moments are given in Eqs. (26), (27) and (28) [30].

$$E_{\text{sw}}(k) = E_{\text{sw\_on}}(k) + E_{\text{sw\_off}}(k) \tag{26}$$

$$E_{\text{sw\_on}}(k) = f_{\text{sw\_on}}(i_{\text{c}}(k)) \tag{27}$$

$$E_{\text{sw\_off}}(k) = f_{\text{sw\_off}}(i_{\text{c}}(k)) \tag{28}$$

With this model designed to calculate the energy losses of semiconductor switches, the accuracy of the PS12038 IPM manufactured by Mitsubishi was calculated by calculating the energy consumption for a certain frequency and power range. For this, the current-voltage loss curves in the datasheet of semiconductor materials to be used in simulation were analyzed and the linearized curves were redrawn in Matlab software. Equations of the obtained functions are obtained by curve fitting methods and the conduction losses of the switches are calculated by obtaining the current-dependent voltage drop values from the equations instantly. The 125 ºC curves in the datasheet were used to obtain the conduction, turn on, turn off and reverse recovery loss equations. Five different equations obtained with Matlab "*polyfit*" tool are given in Eq. (29) as a single equation by decomposing the coefficients.

$$E_{\text{LossType}} = P_1 \cdot x^5 + P_2 \cdot x^4 + P_3 \cdot x^3 + P_4 \cdot x^2 + P_5 \cdot x^1 + P_6 \tag{29}$$

In the given Eq. (26), x is the instantaneous current value of the semiconductor element that will have energy loss. The high degree coefficients obtained for the decoupled energy losses of diode and IGBT of semiconductor materials to be used in simulation are given in Tab. 1. The table shows E_{Qsw_on} for the IGBT switch; turn on, E_{Qsw_off}; turn off, E_{Qcon}; conduction energy losses and for diode E_{Dcon}; conduction, E_{Drr}; reverse recovery represents energy losses. RMSE results of the energy loss equations obtained according to the datasheet of semiconductor components are shared in Tab. 1.

Table 1 High degree coefficients obtained from semiconductor materials with "polyfit" tool in Matlab

Semiconductor Material	Loss Type	Energy Loss Equations Coefficients						Standard Error Deviation
		P_1	P_2	P_3	P_4	P_5	P_6	RMSE
MITSUBISHI IPM PS12038	E_{Qsw_on}	6.13E^{-08}	−6.52E^{-03}	2.80E^{-05}	−464.5E^{-06}	0.1350	2.39	0.03461
	E_{Qsw_off}	5.23E^{-09}	−3.99E^{-07}	7.40E^{-06}	−8.26E^{-05}	0.1500	2.35	0.04263
	E_{Qcon}	3.12E^{-05}	−0.00441	0.0002381	−0.00634	0.1539	0.7429	0.02058
	E_{Dcon}	1.27E^{-09}	−1.49E^{-07}	2.20E^{-05}	−3.03E^{-05}	0.0220	0.65	0.02046
	E_{Drr}	2.10E^{-08}	−3.52E^{-06}	2.14E^{-05}	−6.12E^{-04}	0.1520	0.03	0.02046
SEMIKRON SK75GARL065E	E_{Qsw_on}	−0.01148	0.00814	0.06247	0.27650	1.2610	2.056	0.06715
	E_{Qsw_off}	0.03436	0.00316	−0.20530	0.33020	1.7590	2.741	0.02142
	E_{Qcon}	0.1105	−0.3086	0.09527	0.22810	0.4814	1.71	0.06715
	E_{Dcon}	0.13390	−0.28780	−0.04434	0.24950	0.1787	1.233	0.08945
	E_{Drr}	0.02317	−0.03233	−0.01224	−0.24050	0.9318	2.236	0.02968
IXYS IXSN 80N60AU1	E_{Qsw_on}	0.36860	1.06100	−0.58540	−1.07900	6.3110	9.257	0.09489
	E_{Qsw_off}	−0.12350	0.14390	0.24500	−0.19690	6.0350	10.18	0.10710
	E_{Qcon}	0.26310	−0.63460	0.05160	0.53230	0.4678	2.021	0.01785
	E_{Dcon}	0.02698	−0.05101	−0.01820	0.03039	0.1745	1.432	0.14810
	E_{Drr}	0.00695	−0.02366	0.01686	−0.03965	0.5888	1.293	0.01807

Energy losses were obtained by processing the datasheet of Mitsubishi company's PS12038 IPM power module into the simulation model prepared to calculate the energy losses of semiconductor elements in detail. To measure the accuracy of the results, the results obtained with the Melcosim simulator produced by the same company were compared and presented in Tab. 2. While obtaining the accuracy table, sinusoidal PWM was preferred for the inverter and the power factor was chosen 0.8. Energy loss values of PS12038 semiconductor power module under different loads and frequencies were obtained with the model prepared in Matlab/Simulink. These values are like the Melcosim simulator with a difference of 7.13%. Thus, it is seen that the developed loss calculation method can calculate the switching losses with an acceptable error. With the developed switching loss calculation method, it is possible to compare the switching method developed for the PRDCL inverter with the losses in the calculation of switching losses and other switching methods. The Melcosim software produced by Mitsubishi has been tested and approved in simulator studies on many samples. Therefore, simulator can be considered as a reference. In addition, there are other studies in the calculation of switch energy losses in the literature [32-34].

Table 2 Comparison of energy loss calculation of PS12038 IPM module with melcosim

f_{sw} / W	V_{DC} / V	$I_{L,max}$ /A	Ptot. Melcosim / W	Ptop. Cal. / W	**Difference / %**
5	600	12.5	96.6	101.65	**5.23**
		25	217.38	232.88	**7.13**
10		12.5	152.52	160.3	**5.1**
		25	318.3	317.62	**−2.14**
15		12.5	208.2	220.41	**5.86**
		25	419.16	438.06	**4.5**

4 SIMULATION RESULTS OF THE SYSTEM WITH SIMULINK

The theoretical analyzed simulation studies of the PRDCL inverter system connected to the grid were performed in Matlab/Simulink. The current at the output of the inverter was filtered with an L-filter, and the grid was represented by three voltage sources with a phase difference of 120° between them. The voltage source DC is obtained by passing the three-phase grid through a high value capacitor after rectification. In the simulations, the power module PS12038 IPM was used for the inverter, for the PRDCL auxiliary circuit (S_{Y1} and S_{Y2}), the serial number SK75GARL065E from Semikron and the serial number IXSN 80N60AU1 for the IGBT switch (S_S) connected in series with the DC bus. In the prepared model, the dq-PLL method for grid synchronization and the switching control of the inverter are performed using the sinusoidal PWM (SPWM) technique. The control of the PRDCL structure is provided by using the proposed switching technique. The circuit element values and nominal operating conditions used for the simulation study are listed in Tab. 3.

Table 3 Simulation parameters of model

	Circuit Element	Value	Unit
Grid Connected Inverter Parameters	Grid Voltage (phase-phase)	380	Vrms
	DC-Link Voltage	600	V
	Rectifier Capacitor	1500	µF
	Fundamental Frequency (f)	50	Hz
	Phase Reactor	3	mH
	Phase Resistance	0.12	Ω
Auxiliary Circuit PRDCL Parameters	Resonant Inductance	80	µH
	Resonant Capacitor	40	nF
	Switching Frequency (f_S)	5-10-15	kHz

Figs. 6 and 7 show the waveform for f_{sw} = 15 kHz of the three-phase current delivered to the grid during hard and soft switching, respectively.

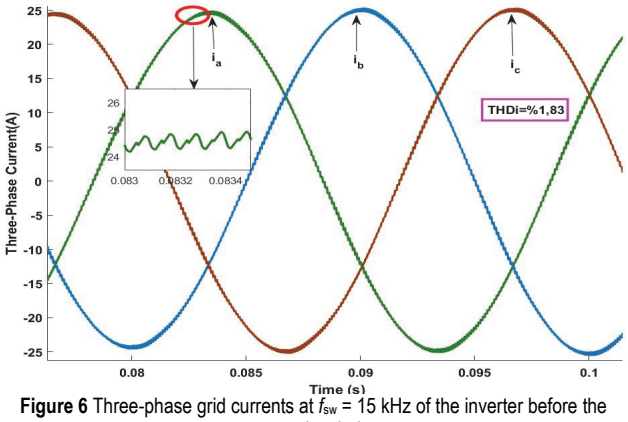

Figure 6 Three-phase grid currents at f_{sw} = 15 kHz of the inverter before the proposed technique

FFT analysis of the current waveform is required to detect the degree of distortion of the current transmitted to the grid. According to the simulink FFT analysis, the THDi value of the current was 1.83% before the application, while it increased to 4.12% after the application. The results obtained show that the current distortion level is less than the limit specified in the standards IEEE -519.

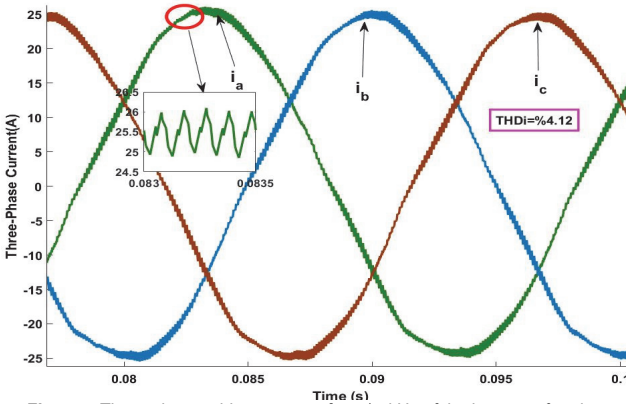

Figure 7 Three-phase grid currents at f_{sw} = 15 kHz of the inverter after the proposed technique

There are two main parameters that cause distortion of the current waveform. First, the proposed technique was developed as a digital control method. In this control technique, the pulse signals sent to the inverter switches are delayed. The delayed switching signals have a negative effect on the formation of reference currents because they partially delay the current to be generated for the grid. The second reason lies in the analog part of the proposed control technique. In order to generate the zero voltage required for soft switching, the capacitor voltage is reduced to zero at each switching. Although very small time frames (µsn) are involved, this can still have a negative effect on the THDi value.

Before applying the technique, the graphs of the current and voltage fluctuations of the inverter switch of the hard circuit are shown in Fig. 8. In order for the switching technique to hardly switch the inverter switches in a safe and healthy manner, the gate pulses applied to the auxiliary switches must be given at appropriate times according to the design criteria. Improper or uncontrolled application of pulses to the gates may result in excessive current in the resonant inductance and subsequently damage the elements.

The current-voltage diagrams of the inverter's main switch S_1 and auxiliary switches S_{Y1} and D_1 when using the soft-switching technique are shown in Figs. 9, 10 and 11. Fig. 8 shows that the current-voltage overlaps are higher with hard-switching of inverter switches. In high frequency regions, these overlaps cause higher energy losses. Applying the proposed technique to the inverter, it can be seen in Figs. 9, 10 and 11 that all switches are soft switched.

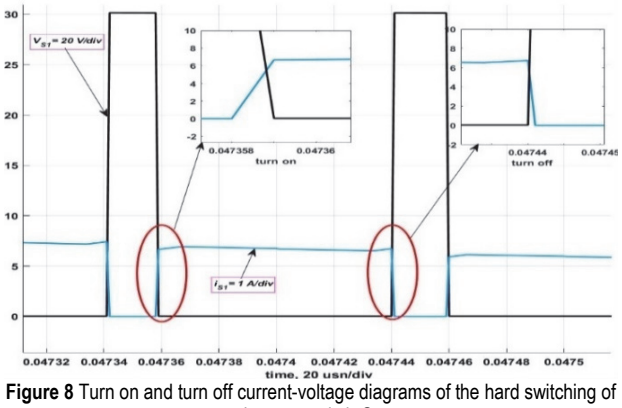

Figure 8 Turn on and turn off current-voltage diagrams of the hard switching of inverter switch S_1

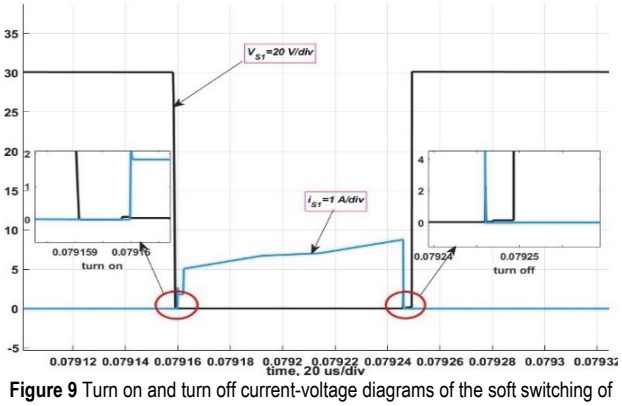

Figure 9 Turn on and turn off current-voltage diagrams of the soft switching of auxiliary switch S_1

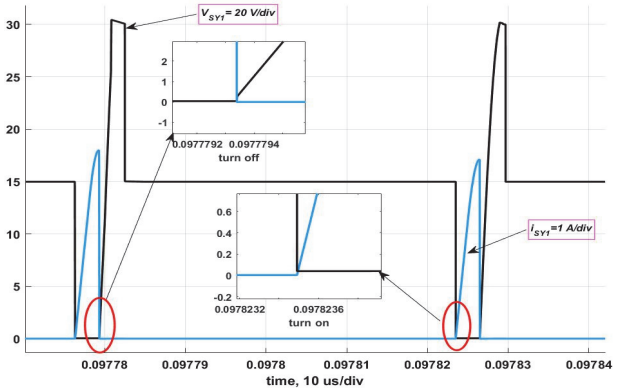

Figure 10 Turn on and turn off current-voltage diagrams of the soft switching of auxiliary switch S_{Y1}

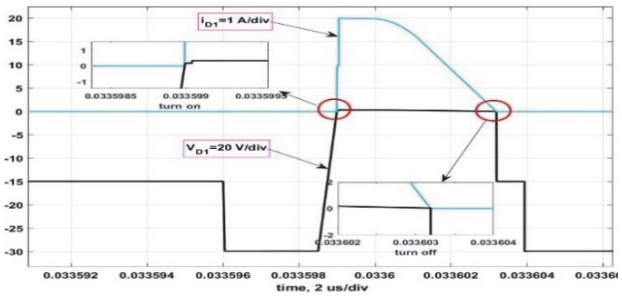

Figure 11 Turn on and turn off current-voltage diagrams of the soft switching of auxiliary diode D_1

In the simulation results: When 5 kW of power is transferred to the grid at a switching frequency of 5 kHz, the total power dissipation of the inverter is 101.65 W for hard switching, while this value decreases to 56.7 W for soft switching. When 10 kW power is transmitted to the grid, the power dissipation is 232.88 W for hard switching, while this value decreases to 138.4 W for soft switching. Moreover, when 5 kW power is transferred to the grid at a switching frequency of 10 kHz, the inverter power dissipation is 160.3 W for the hard switching and 59 W for the soft switching, while these values are 317.62 W and 141.05 W, respectively, for 10 kW power transfer. According to the efficiency curves obtained, an increase in efficiency was achieved at both half and full load.

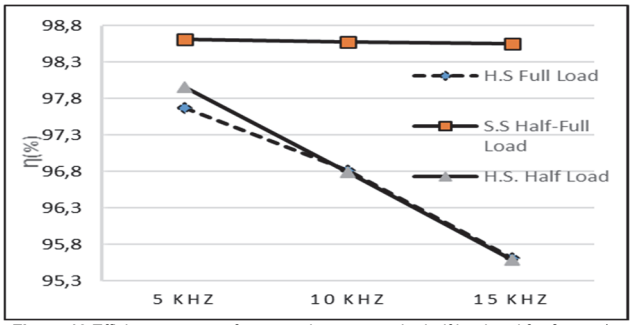

Figure 12 Efficiency curves of proposed system under half load and for f_{sw} = 5-15 kHz range

From the results at half load shown in Fig. 12, it can be seen that the efficiency increases with increasing frequency. This increase is 0.9% for 5 kHz, 2.03% for 10 kHz and 3.15% for 15 kHz. Unlike the half load, it caused a lower efficiency increase in the high frequency regions at full load. As follows; 0.94% for 5 kHz, 1.76% for 10 kHz and 2.94% for 15 kHz were obtained. Since the upper limit of the operating frequency of the selected inverter module is 15 kHz, it could not be tested at higher frequencies.

The comparative data of the proposed soft switching control techniques for different inverters and the proposed switching control technique in terms of cost, performance and control structure are given in Tab. 4.

Table 4 Comparison of different soft switching control techniques

Ref.	Control Type	Sensor Quant.	Control Structure	Cost	MCU proces time	Eff. Gain
[16]	Digital	0	Very Simple	Cheap	Short	3.0%
[24]	Digital	0	Comp.	Exp.	Short	3.3%
[35]	Analog-Digital	2	Comp.	Exp.	Long	2.0%
Proposed tech.	Digital	0	Very Simple	Very Cheap	Very Short	3.15%

5 CONCLUSIONS

In this study, a new switching technique is proposed for PRDCL inverter which belongs to soft switching topologies. The operation of the proposed switching technique and the control infrastructure are explained and simulated in a system connected to a three-phase grid. In the simulation studies, it can be observed from the obtained current-voltage waveforms that both the main and auxiliary switches can switch on and off softly. While ZVT and ZCT occur in the inverter switches, ZVS and ZCS are observed in the auxiliary switches and diodes. This helps to increase efficiency by reducing energy losses. According to the results, the proposed system efficiency and grid current THDi value are measured as 98.86% and 4.12%, respectively. The most efficient condition of the proposed system was measured when transmitting 5 kW at a frequency of 15 kHz to the grid, and the efficiency increase was 3.15%. Moreover, when transmitting 10 kW to the grid, the efficiency increase was 2.94% at the same frequency.

Abbreviations

APF - active power filter
PLL - phase looked loop
PF - power factor
HS - hard switching
SS - soft switching
ZCS - zero current switching
ZCT - zero current transition
ZVS - zero voltage switching
ZVT - zero voltage transition
RPI - resonant pole inverter
PWM - pulse with modulation
RDCLI - resonant dc link inverter
DPM - discrete pulse modulation
QRDCL - quasi dc link inverter
PRDCL - parallel resonant dc link
IPM - intelligent power module
RMSE - root mean square error

Acknowledgements

This study was conducted for the project code ENGINEERING.19002 supported by the Dicle University Scientific Research Project (DUBAP) unit. The authors thank DUBAP for their contribution to this project.

6 REFERENCES

[1] Characteristic of the Utility Interface for Photovoltaic (PV) Systems, IEC Standard 1727, 2002.

[2] Kan, J., Xie, S., Wu, Y., Tang, Y., Yao, Z., & Chen, R. (2015). Single-stage and boost-voltage grid-connected inverter for fuel-cell generation system. *IEEE Transactions on Industrial Electronics*, *62*(9), 5480-5490. https://doi.org/10.1109/TIE.2015.2416339

[3] Xingkui, M., Qisheng, H., Qingbo, K., Yudi, X., Zhe, Z., & Andersen, M. A. E. (2016). Grid-connected photovoltaic micro-inverter with new hybrid control LLC resonant converter. *47th Annual Conference of the IEEE Industrial Electronics Society*, 2319-2324. https://doi.org/10.1109/IECON.2016.7793632

[4] Timbus, A., Teodorescu, R., Blaabjerg, F., & Liserre, M. (2005). Synchronization methods for three phase distributed power generation systems an overview and evaluation. *IEEE Power Electronics Specialists Conference (PESC'05)*, 2474-2481. https://doi.org/10.1109/PESC.2005.1581980

[5] Guo, X., Weiyang, W., Sun, X., & Guocheng, S. (2008). Phase locked loop for electronically-interfaced converters in distributed utility network. *International Conference on Electrical Machines and Systems (ICEMS'08)*, 2346-2350.

[6] Kim, J. W. & Kim, H. G. (2006). Digital PLL control for single-phase photovoltaic system. *IEE Electric Power Applications*, *153*(1), 40-46. https://doi.org/10.1049/IP-EPA:20045225

[7] Svensson, J. (2001). Synchronisation methods for grid-connected voltage source converters. *IEE Generation, Transmission and Distribution*, *148*(3), 229-235.

https://doi.org/10.1049/ip-gtd:20010101.
[8] Saccomando, G. & Svensson, J. (2001). Transient operation of grid-connected voltage source converter under unbalanced voltage conditions. *IEEE Industry Applications Conference*, 2419-2424. https://doi.org/10.1109/IAS.2001.955960
[9] Genc, F. (2008). *Analysis of soft-switching techniques in inverters and implementation of an application circuit*. Master's Thesis, Yıldız Technical University, Graduate School of Science and Engineering, Istanbul.
[10] Divan, D. M. & Skibinski, G. (1987). Zero switching loss inverters for high power applications. *IEEE IAS*. https://doi.org/10.1109/28.31240.
[11] Gokbulut, A. S. (2001). *Three phase resonant circuit inverter*. Master's Thesis, Yıldız Technical University, Graduate School of Science and Engineering, Istanbul.
[12] Aksoy, I. (2001). *Resonant DC links with zero voltage transition*. Master's Thesis, Yıldız Technical University, Graduate School of Science and Engineering, Istanbul.
[13] Obdan, H. (2002). *Improvement of a new resonant DC link inverter for induction motor control and implementation of an application circuit*. PhD Thesis, Yıldız Technical University, Graduate School of Science and Engineering, Istanbul.
[14] Behzadpour, K. & Amini, M. R. (2019). Applying a novel soft switching technique to three-phase active power filter. *8th International Conference on Renewable Energy Research and Applications*. https://doi.org/10.1109/ICRERA47325.2019.8996910
[15] Yeh, C. S., Chen, C.W, Lee, M., & Lai, J. S. (2020). A hybrid modulation method for single-stage soft switching inverter based on series resonant converter. *IEEE Transactions on Power Electronics*, *35*(6). https://doi.org/10.1109/TPEL.2019.2948122
[16] Amini, M. R. & Farzanehfard. H. (2011). Three-phase soft-switching inverter with minimum components. *IEEE Transactions on Industrial Electronics*, *58*(6). https://doi.org/10.1109/TIE.2010.2064280
[17] Cho, J. G., Kim, H. S., & Cho, G. H. (1991). Novel soft switching pwm converter using a new parallel resonant DC-link. *Power Electronics Specialists Conference, PESC '91 Record, 22nd Annual IEEE*, 241-247. https://doi.org/10.1109/PESC.1991.162683.
[18] Fazlali, B. & Adib, E. (2017). Quasi-resonant DC-link H5 PV inverter. *IET Power Electron*ics, *10*(10), 1214-1222. https://doi.org/10.1049/iet-pel.2016.0970
[19] Turzynski, M., Chrzan, P. J., Kolincio, M., & Burkiewicz, S. (2017). Quasiresonant DC-link voltage inverter with enhanced zero-voltage switching control. *2017 19th European Conference on Power Electronics and Applications (EPE'17 ECCE Europe).* https://doi.org/10.23919/EPE17ECCEEurope.2017.8099289
[20] Kedarisetti, J. & Mutschler. P. (2012). A motor-friendly quasi-resonant DC-link inverter with lossless variable zero-voltage duration. *IEEE Transactions on Power Electronics*, *27*(5), 2613-2622. https://doi.org/10.1109/TPEL.2011.2174382
[21] Chu, E., Xie, H., Chen, Z., Bao, J., Zhou, Y., & Zhang, H. (2020). Parallel resonant DC link inverter topology and analysis of its operation principle. *IEEE Journal of Emerging and Selected Topics in Power Electronics*, *8*(3). https://doi.org/10.1109/JESTPE.2019.2914482
[22] Wu, W., Wang, X. L., Geng, P., & Tang, T. (2008). Efficiency analysis for three phase grid-tied PV inverter. *IEEE International Conference on Industrial Technology (ICIT'08)*, *1*(5). https://doi.org/10.1109/ICIT.2008.4608347
[23] Graovac, D., Pürschel, M., & Kiep, A. (2006). MOSFET power losses calculation using the data-sheet parameters. *Application Note*, *1.1*.
[24] Kou, B., Wei, J., & Zhang, L. (2020). Switching and conduction loss reduction of dual-buck full-bridge inverter through ZVT soft-switching under full-cycle modulation. *IEEE Transactions on Power Electronics*, *35*(5). https://doi.org/10.1109/TPEL.2019.2943700
[25] IEEE 519-1992 Standard, IEEE Recommended Practices and Requirements for Harmonic Control in Electrical Power Systems.
[26] Donuk, H. & Gümüş, B. (2021). Hardware in the loop(hil) matlab/simulink co-simulation of shunt active power filter. *Journal of Polytechnic*, *1*(1). https://doi.org/10.2339/politeknik.938480
[27] Song, S. H., Kang, S. I., & Hahm, N. K. (2003). Implementation and control of grid connected AC-DC-AC power converter for variable speed wind energy conversion system. *IEEE Applied Power Electronics Conference and Exposition (APEC '03)*, 154-158. https://doi.org/10.1109/APEC.2003.1179207
[28] Malinowski, M. & Bernet, S. (2004). Simple control schme of three-level PWM converter connecting wind turbine with grid. *International Conference on Renewable Energies and Power Quality (ICREP'04).* https://doi.org/10.24084/repqj02.215
[29] Lai, J. S. & Bose, B. K. (1988). An improved resonant DC-link inverter for inductıon motor drives. *IEEE IAS*, 742-748. https://doi.org/10.1109/IAS.1988.25145
[30] Zhou, Z., Khanniche, M. S., Igic, P., Kong, S. T., & Towers, M. (2005). A fast power loss calculation method for long real time thermal simulation of IGBT modules for a three-phase inverter system. *European Conference on Power Electronics and Applications (EPE'05)*, 9-10. https://doi.org/10.1109/EPE.2005.219598
[31] Akagi, H. (1996). New trends in active filters for power conditioning. *IEEE Transactions on Industry Applications*, *32*(6). https://doi.org/10.1109/28.556633
[32] Isen, E. & Bakan, A. F. (2018). Highly efficient three-phase grid-connected parallel inverter system. *Journal of Modern Power Systems and Clean Energy*, 1079-1089. https://doi.org/10.1007/s40565-018-0391-7
[33] Plakhtii, O. A, Nerubatskyi, V. P, Hordiienko, D. A., & Tsybulnyk, V. R. (2019). Analysis of the energy efficiency of a two-level voltage source inverter in the overmodulation mode. *Naukovyi Visnyk Natsionalnoho Hirnychoho Universytetu*. https://doi.org/10.29202/nvngu/2019-4/9
[34] Patel, A., Joshi, S., Chandwani, H. B., Patel, V., & Patel, K. (2010). Estimation of Junction Temperature and Power loss of IGBT used in VVVF Inverter using Numerical Solution from Data sheet Parameter. *International Journal of Computer Communication and Information System*, *2*(1).
[35] Kurokawa, M., Konishi, Y., & Nakaoka, ve M. (2002). Auxiliary resonant DC link snubber assisted voltage-source soft switching inverter with space zero voltage vector generation method. *IEE Proceedings - Electric Power Applications - C*, *149*(5). https://doi.org/10.1049/ip-epa:20020473

Contact information:

Hakan DONUK
(Corresponding author)
Cizre Vocational School, Department of Electronics and Automation,
Şırnak University,
73200 Şırnak, Turkey
E-mail: hakandonuk@sirnak.edu.tr

Bilal GUMUS
Department of Electrical and Electronics Engineering, Faculty of Engineering,
Dicle University,
21280 Diyarbakır, Turkey
E-mail: bilgumus@dicle.edu.tr